Applied Energy 175 (2016) 512–521

Contents lists available at ScienceDirect

Applied Energy

journal homepage: www.elsevier.com/locate/apenergy

# Scalable synthesis of functionalized graphene as cathodes in Li-ion electrochemical energy storage devices

Dongbin Xiong [a,b,c], Xifei Li [a,b,*], Hui Shan [a,b], Bo Yan [a,b], Dejun Li [a,b,*], Craig Langford [d], Xueliang Sun [d,a,b,*]

[a] Energy & Materials Engineering Centre, College of Physics and Materials Science, Tianjin Normal University, Tianjin 300387, China
[b] Tianjin International Joint Research Centre of Surface Technology for Energy Storage Materials, Tianjin 300387, China
[c] Key Laboratory of Advanced Energy Materials Chemistry (Ministry of Education), Collaborative Innovation Center of Chemical Science and Engineering, College of Chemistry, Nankai University, Tianjin 300071, China
[d] Nanomaterials and Energy Lab, Department of Mechanical and Materials Engineering, Western University, London, Ontario N6A 5B9, Canada

## HIGHLIGHTS

- The functionalized graphene nanosheets (FGNS) were synthesized.
- The functionalized graphene cathode showed high specific capacity and excellent cyclability.
- Oxygenic functional groups act as active sites for lithium storage.
- The proposed route exhibited some promising possibilities for mass production.

## GRAPHICAL ABSTRACT

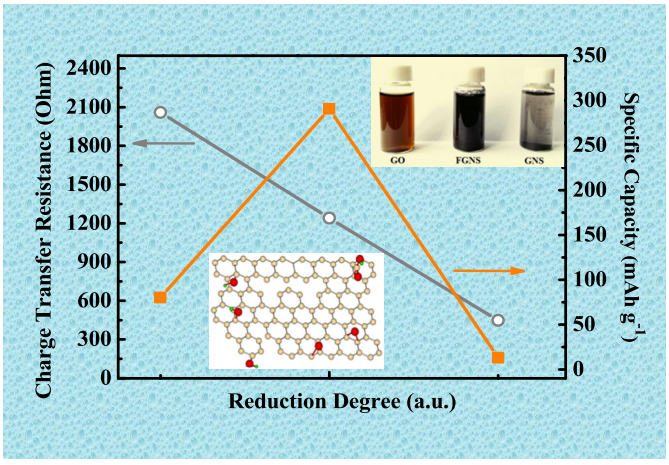


## ARTICLE INFO

*Article history:*
Received 25 December 2015
Received in revised form 2 March 2016
Accepted 28 March 2016
Available online 9 April 2016

*Keywords:*
Solvothermal reduction
Graphene
Oxygenic functional groups
Lithium ion batteries
Cathode materials

## ABSTRACT

It is highly desirable to develop high-performance and cost-effective cathode materials for lithium-ion batteries (LIBs). In this work, functionalized graphene nanosheets (FGNS) were facilely synthesized utilizing ethylene glycol as both reducing agent and solvent. When employed as cathode materials for LIBs, FGNS were demonstrated to exhibit superior electrochemical performance when compared with traditional metal oxide-based cathodes. For instance, FGNS deliver outstanding cycle stability and high specific discharge capacity of 280 mA h $g^{-1}$ at 0.05 A $g^{-1}$ without obvious capacity fading after 300 cycles. Furthermore, FGNS reveal high rate capacity of 152 mA h $g^{-1}$ at a high current density of 0.4 A $g^{-1}$. The excellent electrochemical performance is attributed to the oxygen-containing functional groups and specific poriferous structure of FGNS. The proposed FGNS are expected to be a simple, low-cost, efficient, and large-scale production of cathode materials for LIBs.

© 2016 Elsevier Ltd. All rights reserved.

* Corresponding authors at: Energy & Materials Engineering Centre, College of Physics and Materials Science, Tianjin Normal University, Tianjin 300387, China (X. Li). Tel.: +86 22 23766526; fax: +86 22 23766503.
*E-mail addresses:* xfli2011@hotmail.com (X. Li), dejunli@mail.tjnu.edu.cn (D. Li), xsun9@uwo.ca (X. Sun).

http://dx.doi.org/10.1016/j.apenergy.2016.03.105
0306-2619/© 2016 Elsevier Ltd. All rights reserved.

## 1. Introduction

Energy conservation and environment protection have become important topics in the energy field. During various sustainable devices for energy storage and conversion, secondary lithium ion batteries (LIBs) with high energy density, long circle life and environmentally benign characteristics are highly desired as potential power sources for portable electronic devices, electric vehicles (EV) and smart electricity grid [1–4]. But the current LIB technology does not satisfy the increasing demand of miniaturization of power sources for electronic devices and does not address the need for faster charging electric vehicles, especially current electric vehicles utilizing LIBs as power source are hindered by short range and long charging time, which degrades the user experience and hinders the large-scale development of EV [5,6]. To increase the capacity, lifecycle, and rate capability of LIBs, strategies include to improvement of the current electrode materials as well as proposing new cathode materials for the next generation rechargeable LIBs with high performance [7]. The attractive merit is that the commercial graphite anode actually delivers the high energy capacity of more than 330 mA h $g^{-1}$ (372 mA h $g^{-1}$ theoretically) [8,9]. However, the common inorganic intercalation cathode materials (e.g., $LiCoO_2$, $LiFePO_4$ or $LiNi_{1/3}Co_{1/3}Mn_{1/3}O_2$) reveal some severe drawbacks such as low practical capacity (~170 mA h $g^{-1}$) in all cases, unreliable safety in the case of $LiCoO_2$, as well as the relatively high cost of cobalt (Co) and limited mineral resources for $LiCoO_2$ and $LiNi_{1/3}Co_{1/3}Mn_{1/3}O_2$ [5,10]. As a result of the low capacity, the incorporation of the cathode material is always double the anode material, which limits further improvement of battery performance. Therefore, so far, to significantly improve the cathode performance has been proven to be a challenge. Recently, three-component layered oxide systems in the form of $LiNi_xCo_yMn_zO_2$ (NCM, $0 \leqslant x, y, z < 1$) and Ni-based layered oxide systems in the form of $LiNi_{1-y-z}Co_yAl_zO_2$ (NCA, $0 \leqslant y, z < 1$) have exhibited promising alternatives as cathode materials to substitute for $LiCoO_2$, but for long-term cycling, some problems such as electrolyte decomposition and dissolution of transition metals occur at the electrode–electrolyte interface, which will lead to poor cycling stability and uncontrolled voltage changes [11–14]. For instance, the $LiNi_{0.8}Co_{0.15}Al_{0.05}O_2$ studied shows limited applications in EV systems owing to its poor rate capability as well as poor stability in a high temperature environment of 55 °C [15]. Another developmental layered Li-rich materials can deliver a reversible capacity of more than 200 mA h $g^{-1}$ when charged to 4.5 V, but they suffer from obvious voltage changes and inferior rate capability upon cycling [16]. Hence, new advanced cathode materials that demonstrate high reversible capacity while having superior cycling stability and low-cost are highly desirable.

Recently, the proposed replacement of the lithium metal oxide cathodes by graphene may, in principle, allow high cycling stability of Li electrochemical storage devices with high energy and power density [17,18]. High aspect ratio, good electrical conductivity and high surface area of the two-dimensional structure of graphene nanosheets [19,20] contribute to enhancing electrochemical performance when employed as cathode materials for both LIBs and supercapacitors [21–23]. A host of studies have demonstrated the pivotal role of oxygenic functional groups, which serve as active sites for lithium storage during the charge–discharge process based on the electrochemical reaction: $\rangle C{=}O + Li^+ + e^- \leftrightarrow \rangle C{-}O{-}Li$ [23–28]. Both organic cathode materials, typically organic carbonyl compounds, and graphene-based cathode materials, such as reduced graphene oxide and functionalized carbon nanotubes [29–31], deliver higher energy capacities than inorganic metal oxide cathodes [32,33]. Unfortunately, organic cathodes show poor electrochemical performances due to their poor electrical conductivity and chemical stability in the electrolyte, which provides organic cathodes less superiority when compared with lithium metal oxide cathodes. Graphene-based cathode materials, on the other hand, exhibit great potential as transition-metal-free and cost-effective cathodes due to excellent cycling stability and high energy density/power density. However, as previously reported, the synthesis of a functionalized graphene cathode is generally based on tedious chemical reduction with low yields, such as annealing in specific atmosphere [25,34], or with a selective reduction in the organic solvent but with a relatively low energy density [35], which shows some difficulties in scale-up of the promising cathode materials.

In this study, we present a novel strategy for the fabrication of functionalized graphene nanosheets (FGNS) by partial reduction of the oxygenic functional groups of graphene oxide (GO). The FGNS proved to be superior cathode materials, which manifests high Li storage properties, superior rate capability and excellent cycling stability. The enhanced electrochemical performance was mainly owing to the lithium storage capacity of abundant oxygenic functional groups on the planes or edges of graphene nanosheets together with a highly conductive poriferous graphene framework. It is worth noting that during the process of partial reduction, nontoxic and low-cost ethylene glycol was used as a reducing agent and solvent at low temperature of ~120 °C, and during the separation of final product and cheap-nontoxic reductant, physical sedimentation method was adopt instead of other complicated methods such as filtration and centrifugation. Therefore, this proposed facile method shows some promising possibilities for mass production, and opens an opportunity to develop this potential cathode materials a new cathode material for high performance LIBs.

## 2. Experimental

### 2.1. Chemicals

Natural graphite powder (purity ⩾ 99.95%) was supplied by the Aladdin Chemistry Co., Ltd. Concentrated sulfuric acid (95–98%), fuming nitric acid (65–68%), $KMnO_4$ (99%), $NaNO_3$ (99%), $H_2O_2$ (30%) and ethylene glycol (99.5%) were used as received from Tianjin Jiangtian Chemical Research Institute.

### 2.2. Materials synthesis

First, graphite oxide (GO) was prepared from natural graphite by a modified Hummers' method as reported in our previous work [36]. Next, FGNS was synthesized using GO as raw material and ethylene glycol as solvent agents. In a typical process, 2 mg $mL^{-1}$ solution (100 mL) of graphene oxide in ethylene glycol was made from GO by ultrasonic cell disruption for 40 min. The obtained graphene oxide dispersion was then subjected to centrifugation at 10,000 rpm for 30 min to remove some non exfoliated GO (usually no more than 3 wt.%). The obtained dispersion was then transferred into a 150 mL beaker followed by heating at 120 °C with an oil bath for 12 h under vigorous stirring. After the reaction mixture was naturally cooled down to room temperature, the reaction mixture was subsequently poured into plenty of water to obtain black deposit. The resultant black precipitation was then repeatedly washed with deionized water, and finally the obtained black precipitation was freeze-dried to obtain FGNS. Dried FGNS powder was then charged into a quartz tube and annealed under Ar/5%$H_2$ atmosphere at 900 °C for 2 h with a heating rate of 10 °C $min^{-1}$, the obtained product with removal of the most residual oxygenic functional groups was marked as GNS.

### 2.3. Materials characterization

X-ray diffraction (XRD) spectra were measured using a Bruker AXS D8 Advance diffractometer with Cu/Kα radiation. Fourier-transform infrared spectroscopy (FT-IR) was recorded with an IRAffinity-1 spectrometer. Raman spectra were carried out on a LabRAM HR800 Raman microscope (HORIBA, Korea) in the range of 1000–2000 $cm^{-1}$. The morphology of the prepared samples was observed with field-emission scanning electron microscope (SEM Hitach SU8010) and high-resolution transmission electron microscopy (HR-TEM, JEM-3000F). X-ray photoelectron spectroscopy (XPS) (ESCALAB MK II) was used to investigate the surface chemistries of the obtained materials.

### 2.4. Electrochemical test

Electrochemical performances were investigated by using CR2032 coin-type cell assembled in an argon filled glove box. A metallic lithium foil was used as the reference and counter electrode. The work electrodes were made with active materials, acetylene black and polyvinylidene fluoride binder (PVDF) with a weight ratio of 8:1:1 in N-methyl-2-pyrrolidone (NMP) solvent. Then the resulting slurry was equably pasted onto Al foil and dried in a vacuum oven at 90 °C overnight. The cells were assembled with 1 M $LiPF_6$ dissolved in ethylene carbonate (EC), dimethyl carbonate (DMC) and ethylene methyl carbonate (EMC) (1:1:1 by volume) as the electrolyte. Galvanostatic charge and discharge tests were conducted on LAND CT2001A test system. Cyclic voltammetry was carried out on a Princeton Applied Research Versa STAT 4 electrochemical workstation with a scan rate of 0.1 mV $s^{-1}$. Electrochemical impedance spectroscopy (EIS) tests were conducted on the electrochemical workstation within a frequency range of 0.01–100 kHz with the AC amplitude of 5.0 mV at the full charge state (4.5 V) after the 5th cycle. All the tests were conducted within the potential range of 1.5–4.5 V.

## 3. Results and discussion

The structure and crystal phase information of the samples were obtained by XRD and Raman. Fig. 1(a) shows the XRD patterns of GO, FGNS and GNS. A characteristic diffraction peak of GO at 11.8° is observed, which corresponds to the (001) diffraction peak of GO [37]. The *d*-spacing of GO increases to 0.749 nm from 0.34 nm of graphite (see Fig. S1, before oxidation, the XRD pattern of graphite powder exhibits a characteristic peak of graphite at 26.6°) [38], which is mainly ascribed to the oxide-induced oxygenic functional groups and inserted $H_2O$ molecules [39,40]. After treatment at 120 °C, the (001) diffraction peak disappears, indicating that the GO was successfully reduced into FGNS. The existence of characteristic peaks at 29.2° and 41.5° correspond to (002) and (100) planes, respectively, which demonstrate the removal of oxygenic functional groups and partial recovery of the graphitic structure. The broad peaks indicate that the FGNS is typical of non-graphitic carbon structure with a high degree of disorder [21]. The (002) diffraction peak of GNS at 20.5° indicates that the *d*-spacing of GNS was with further extension. Fig. 1(b) shows the Raman spectra for the obtained GO, FGNS and GNS samples. It is well known that D band corresponds to the structural defects, while G band is a characteristic feature of graphitic layers. The $I_D/I_G$ band intensity ratio indicates the degree of distortion of a graphitic lattice [41,42]. In this study, an obvious G band at 1595 $cm^{-1}$ and a typical D band at 1350 $cm^{-1}$ were observed in three samples. The intensity ratios of D band to G band ($I_D/I_G$) of GO, FGNS and GNS were 1.36, 1.59 and 1.82, respectively. Herein, with the reduction of GO, the $I_D/I_G$ ratio of FGNS and GNS increased gradually, indicating that extensive reduction has led to a substantial decrease of the size of the in-planes $sp^2$ domains, as well as an increase of edge planes and the degree of disorder in the FGNS and GNS [43]. The defects related to disordered carbon structure, such as boundaries, vacancy and amorphous structure, which can provide more active sites for lithium storage, and enhance the electrochemical performance of the GNS materials [39].

SEM and TEM were performed to investigate the morphologies and microstructure of the as-prepared FGNS and GNS samples. As shown in Fig. 2, both low- and high-magnification SEM images show that the FGNS possessed uniform 3-dimensional interconnected porous network with walls consisting of thin layers of small and stacked graphene sheets, and the pore sizes ranging from ~10 nm to several micrometers (Fig. 2(a and b)). After further heating the FGNS at 900 °C for 2 h, as shown in Fig. 2(c and d), the obtained GNS still maintained the 3D network morphology without significant change. For comparison, the morphology of GO was also characterized by SEM (see Fig. S2). The GO sheets were loosely stacked like blocks of foam or sponge. Therefore, after a reduction process, most of the GO has been efficiently exfoliated to ultrathin nanosheets with wrinkled structures, and a 3D interconnected porous framework was obtained. Fig. 3(a and b) and (c and d) shows bright-field HRTEM images of FGNS and GNS, respectively. As-prepared FGNS reveals a feature of wavy and transparent structure. The selected area electron diffraction (SAED) pattern (inset of Fig. 3(a)) shows clear diffraction rings, suggesting the partial honeycomb-like atomic structure and the polycrystalline nature of the FGNS sample [37] despite the generation of defects

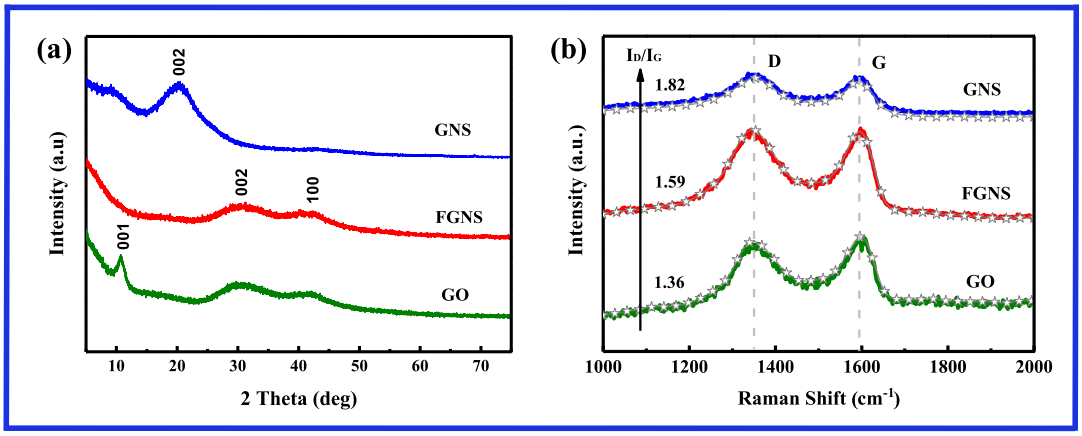


**Fig. 1.** (a) XRD and (b) Raman pattern of the original GO, FGNS and GNS.

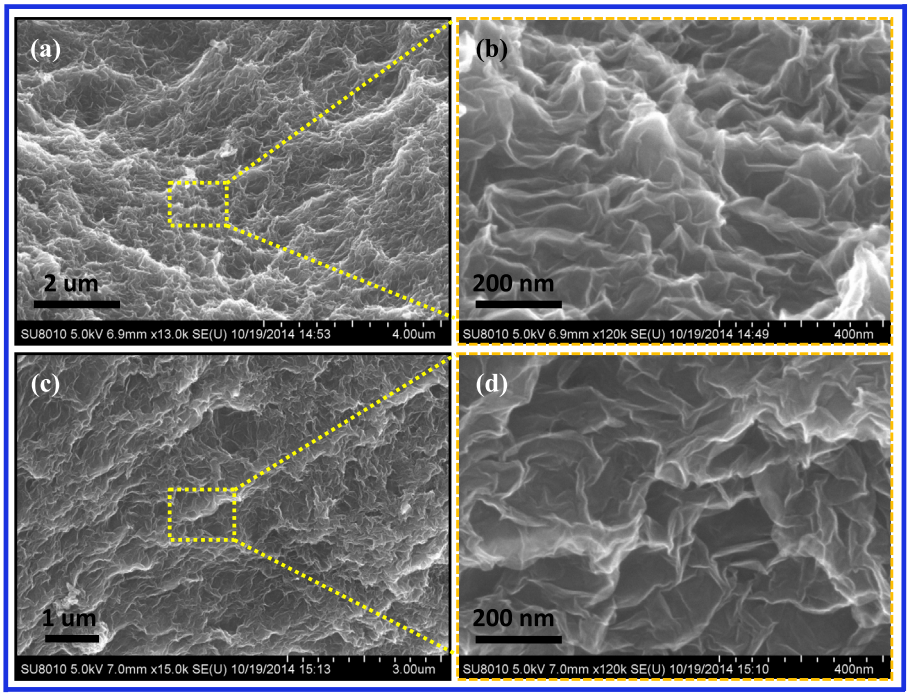


**Fig. 2.** Low- and high-magnification SEM images of the as-synthesized FGNS (a and b) and GNS (c and d).

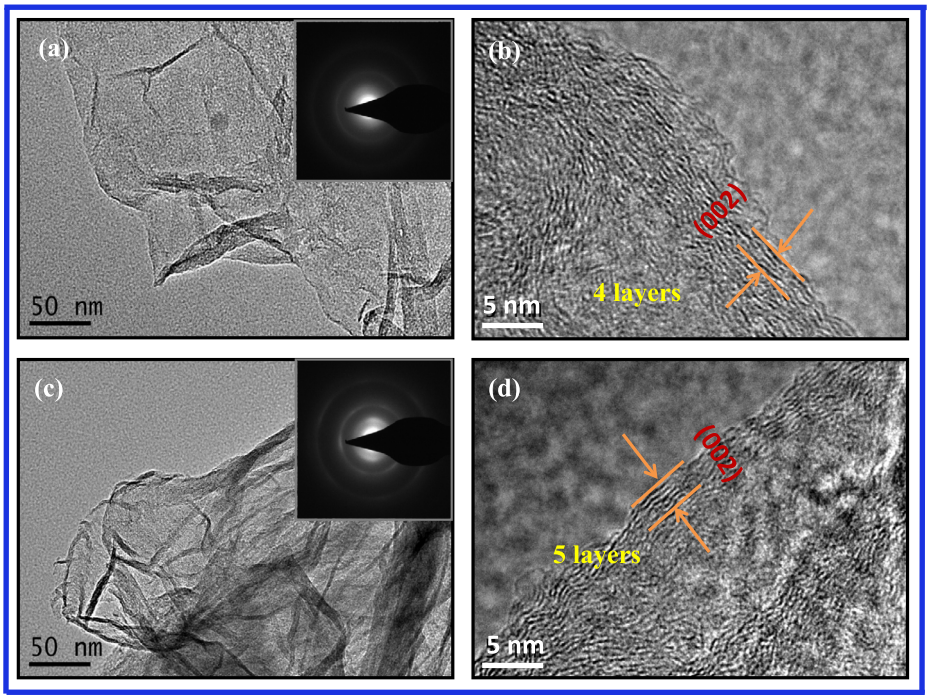


**Fig. 3.** (a and b) TEM images of the as-synthesized FGNS and corresponding SAED pattern (inset of (a)); (c and d) TEM image of the as-synthesized GNS and corresponding SAED pattern (inset of (c)).

such as oxygen-containing groups and vacancies after the chemical oxidation and reduction process. The TEM image of the FGNS edges shows multilayer of graphene with an interlayer distance of 0.32 nm (Fig. 3(b)). This value in $d_{002}$ results from the graphene exfoliation, as well as the decrease of functional groups of GO [44]. After further reduction at 900 °C, the GNS (Fig. 3(c and d)) show similar structure with FGNS, from the SAED pattern (inset of Fig. 3(c)), the defined diffraction rings suggests that vacancies bring more structural irregularity into the hexagonal crystal lattice of GNS, which is highly consistent with the previous XRD and Raman results [45]. Moreover, from the high-magnification TEM image shown in Fig. 3(d), the interlayer spacing of GNS is about 0.35 nm, broader than that of FGNS due to further thermal exfoliation.

XPS studies were performed on FGNS and GNS samples to investigate the elemental composition and chemical status of the

elements. In Fig. 4(a), the survey spectra of the FGNS and GNS samples indicate the incorporation of C and O into these materials. Two characteristic peaks located at 532 and 285 eV were observed, corresponding respectively to O 1s and C 1s [46], respectively. The ratios of O to C of FGNS and GNS were estimated to be 0.303 and 0.025, respectively, indicating that FGNS exhibit obvious characteristic of rich oxygenic functional groups. The bonding configurations of C atoms in FGNS and GNS samples were investigated by high resolution XPS, as displayed in Fig. 4(b and c). The C 1s peak for the two samples could be fitted by several peaks centered at 288.9, 288.1, 286.5 and 284.5 eV. The peaks at 288.9, 288.1, 286.5 and 284.5 eV correspond to the carboxyl groups, the carbonyl groups, the hydroxyl as well as epoxy groups, and the C—C/C=C bonds [47], respectively, and their contents are tabulated in Table 1. The structure model of FGNS is shown in Fig. 4(d). The O 1s spectra of the FGNS and GNS samples (Fig. 4(e)–(f)) reveal that it consists of three components arising from HO—C=O (carboxyl, 533.5 eV), C—O (hydroxyl and epoxy, 532.5 eV) and C=O (carbonyl, 531.6 eV) groups [25], and their contents are tabulated in Table 2. As expected, considerable oxygenic functional groups exist in FGNS, and most of them can be removed after thermal treatment at 900 °C. This can be clearly confirmed by the results in Fig. 4 (c and f) (the total peak intensity in the O 1s regions in Fig. 4(f) is magnified by 4 times).

The FT-IR spectra of the GO, FGNS and GNS are shown in Fig. 5. In the case of GO, many surface oxygenic functional groups are observed. The characteristic absorption peaks appearing at 1730, 1625, 1400, 1225, 1065, and 586 $cm^{-1}$ are attributed to the C=O stretching of the carboxyl groups, C=C stretching (adsorbed water), O—H bending of tertiary CO—OH, CO—O stretching vibrations, C=O stretch of the alkoxy group, and O—H bending of the hydroxyl groups, respectively. Additionally, the strong and broader peak at about 3400 $cm^{-1}$ is related to O—H stretching vibrations [48–51]. These indicated that abundant oxygen-containing groups were successfully created on the surface and edges of GO. Differing from GO, FGNS and GNS show similar FT-IR spectra, in which the

**Table 1**
The C 1s XPS data of FGNS and GNS (relative atomic percentage %).

| Samples | HO—C=O (288.9) (%) | C=O (288.1) (%) | CO—OH (286.5) (%) | CO—C/C=C (284.5) (%) |
|---|---|---|---|---|
| FGNS | 3.48 | 9.17 | 29.81 | 57.54 |
| GNS | 2.02 | 3.73 | 3.94 | 90.31 |

**Table 2**
The O 1s XPS data of FGNS and GNS (relative atomic percentage %).

| Samples | HO—C=O(533.5) (%) | CO—OH(532.5) (%) | C=O(531.6) (%) |
|---|---|---|---|
| FGNS | 36.4 | 37.1 | 26.5 |
| GNS | 43.5 | 30 | 26.5 |

intensities of the peaks related to C=O, O—H and CO—O groups obviously decrease or even disappeared, indicating the successful partial reduction of GO during the solvothermal treatment. It is in good agreement with the XPS results. More importantly, a clear shift of the absorption peaks to a lower wavenumber is observed. Specifically, the absorption peak related to C=O shifts from 1730 to 1710 $cm^{-1}$. It may arise from the conjugation with π bonds which were formed during the recovery of graphene oxide to its graphene form [35,52]. The π bonds will reduce the energy of C=O and make it easy to be broken with more electrochemical activity. Additionally, the shift of C=C/adsorbed water peaks further proves the reduction of GO. The shift of CO—O peak may be due to the different vibration modes after the introduction of vacancy defects [52,53]. Nevertheless, it is worth noting that FGNS exhibits more oxygenic functional groups than GNS, which can be graphically revealed in the schematic diagram of Fig. 4(d).

To explore the electrochemical Li storage behaviors of as-prepared FGNS and GNS as cathodes for LIBs, cyclic voltammetry (CV) and galvanostatic charge–discharge tests were subsequently carried out. The graphite or graphene is generally considered as an anode material owing to its low potential. In this study, the

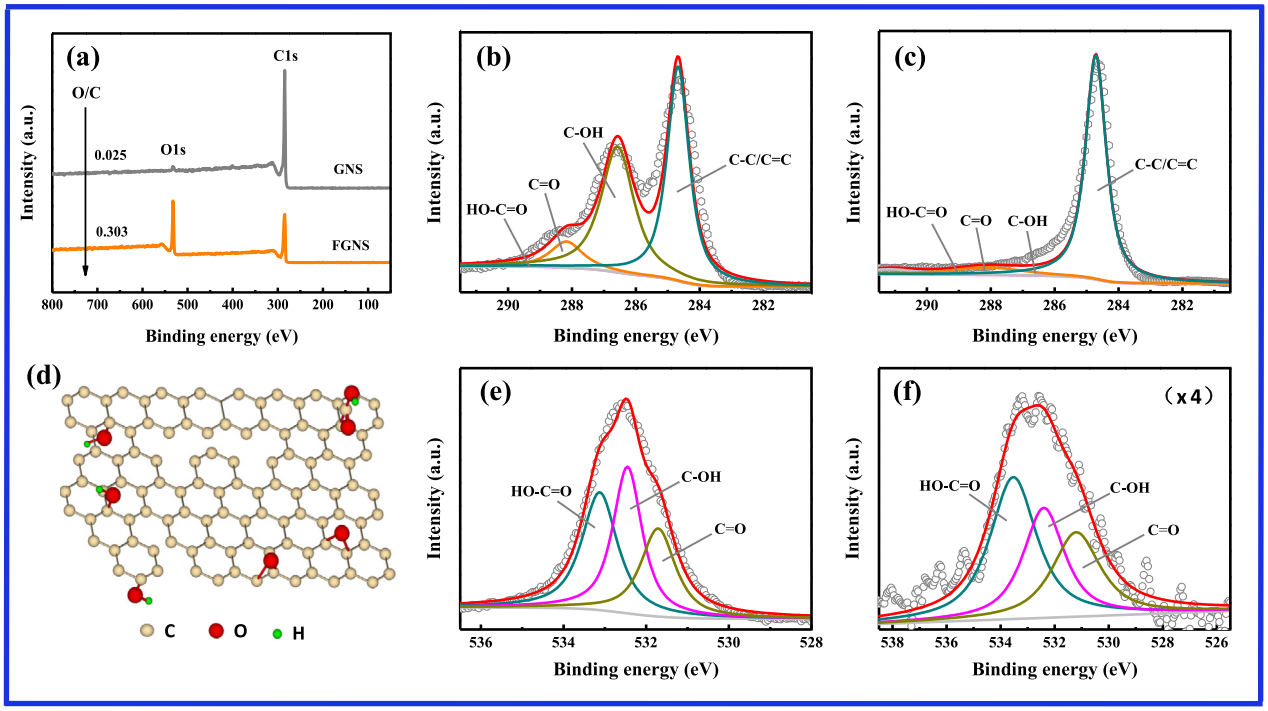


**Fig. 4.** (a) XPS survey spectra of as-synthesized FGNS and GNS; typical C 1s XPS spectra of FGNS (b) and GNS (c); (d) schematic illustration of the structure of FGNS; typical O 1s XPS spectra of FGNS (e) and GNS (f), the intensity of O 1s of the GNS (f) is magnified by 4 times.

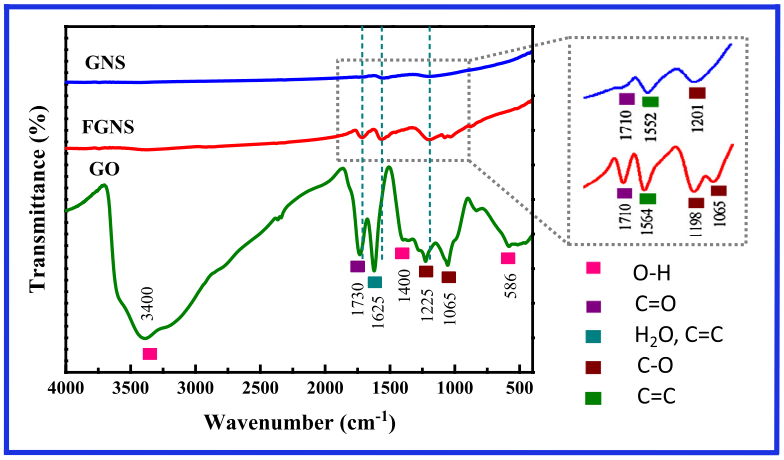


**Fig. 5.** FT-IR spectra of GO, FGNS and GNS.

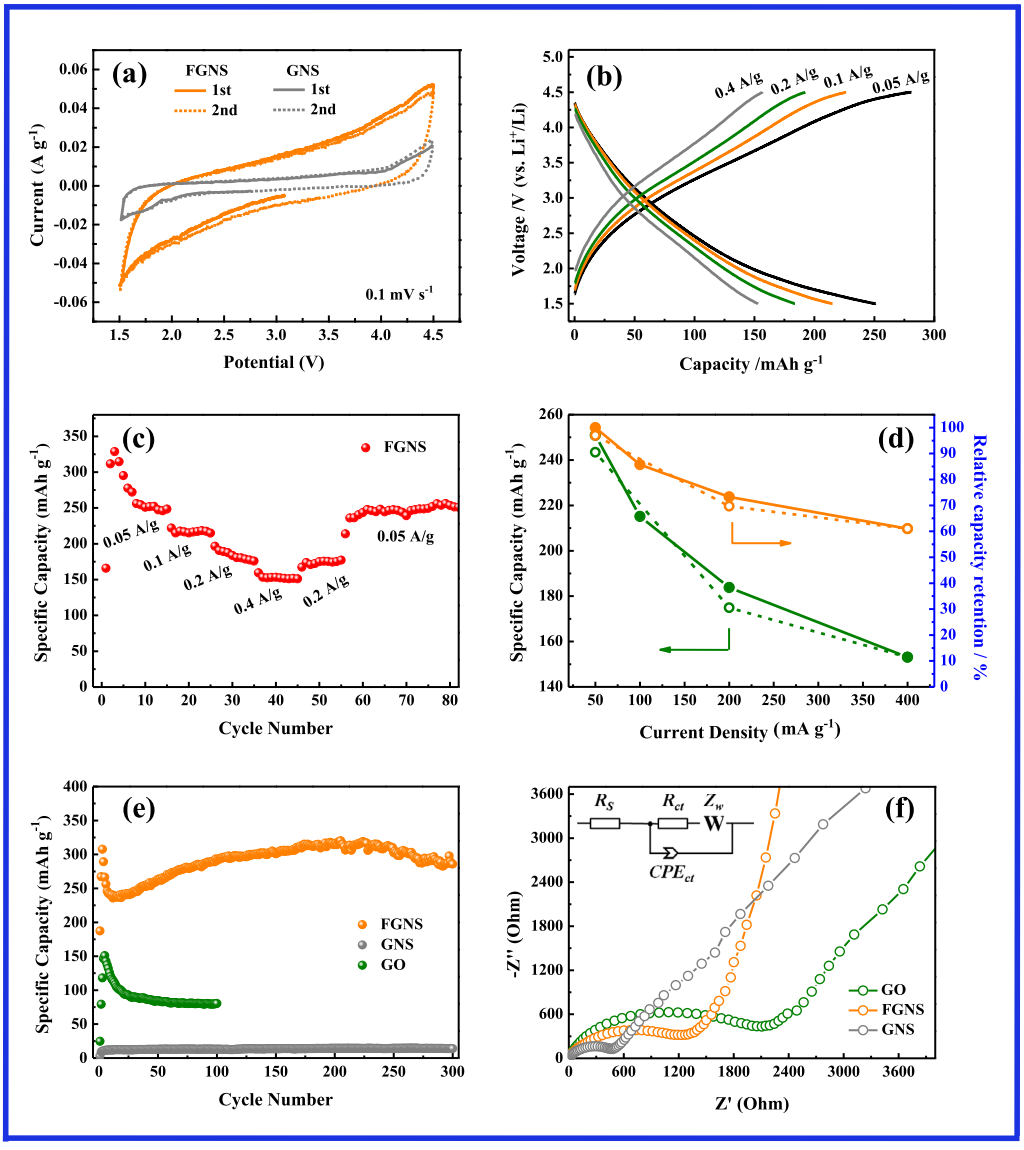


**Fig. 6.** (a) The CV curves of FGNS and GNS at a scan rate of 0.1 mV $s^{-1}$; (b) the charge/discharge profiles of FGNS electrode at various current densities; (c) rate performance of the FGNS electrode; (d) capacity retention of FGNS at different current densities; (e) cycling performance of GO, FGNS and GNS electrodes at a current density of 50 mA $g^{-1}$; (f) the EIS curves of GO, FGNS and GNS samples (inset: the selected equivalent circuit model).

FGNS exhibited a considerably higher operating voltage in the Li cell. As shown in Fig. 6(a), CV measurements of both samples were measured in the voltage range of 1.5–4.5 V (vs. $Li/Li^+$) with a scan rate of 0.1 mV $s^{-1}$. In the first cycles, the open-circuit voltages of the FGNS and GNS were measured to be ~3.08 V and ~2.75 V vs. $Li/Li^+$, respectively. These voltages can be lowered to 1.5 V versus Li to store lithium ions according to the Faradaic reactions of surface functional groups on FGNS and GNS [28,54]. The representative CV curves of the first two cycles of both FGNS show much higher current responses than that of GNS, indicating the surface functional groups are responsible for the electrochemical reactions, which was in good agreement with our previous reports [36,55]. As previously reported, the proposed energy storage mechanism was mainly divided into two parts: (a) the reversible redox reaction of the oxygen functional groups with Li ions, and (b) reversible adsorption and desorption of electrolyte anions (such as $PF_6^-$) on the surface of the graphene nanosheets [23,56]. The schematic illustration in Fig. 7 shows the proposed energy storage mechanism of the proposed FGNS cathode in LIBs: (I) In the initial discharge process, Li ions insert into graphene nanosheets, and are stored by the means of (a) binding to the oxygenic functional groups by breaking double bonds and forming single bonds between carbon and oxygen and (b) adsorbing to the edges or defects of graphene nanosheets. (II) Li ions are removed efficiently by reversible changes of the single to double C—O bonds during the subsequent charge–discharge process, which may ascribe to the higher electroactivity of C=O, as described in FT-IR part. (III) Reversible association and disassociation of electrolyte anions ($PF_6^-$) occur on the nanosheets surface during the charge–discharge process, delivering extra reversible capacity. Herein, for the excellent energy storage performance exhibited, we anticipate that FGNS with considerable functional groups and porous structure holds colossal promise as novel cathode materials for LIBs.

Fig. 6(b) clearly shows the charge and discharge curves of FGNS at various current densities (from 0.05 to 0.4 A $g^{-1}$) with a voltage range from 1.5 to 4.5 V (vs. $Li/Li^+$). The charge and discharge profiles were sloping lines without any apparent voltage plateau corresponding to the CV curves in Fig. 6(a), and this feature is similar to those previously proposed functionalized graphene cathode materials [57,58]. The specific discharge capacities of FGNS cathode were 252, 216, 183 and 153 mA h $g^{-1}$ at a current density of 0.05, 0.1, 0.2 and 0.4 A $g^{-1}$, respectively. The remarkable rate performance was further confirmed in Fig. 6(c). Notably, a high capacity of 253 mA h $g^{-1}$ was restored when the current density was recovered to 0.05 A $g^{-1}$. Fig. 6(d) displays the discharge capacities of the $10^{th}$ cycle at various current densities as well as their capacity retention in comparison to the capacity at 0.05 A $g^{-1}$. When compared to the capacity at 0.05 A $g^{-1}$, the capacity retention percent of FGNS were 85.7%, 72.6% and 60.7% at 0.1, 0.2 and 0.4 A $g^{-1}$, respectively. More importantly, in the $61^{st}$ cycle, the capacity of FGNS cathode can recovered to 97% of the capacity at 0.05 A $g^{-1}$. These results demonstrate that the FGNS show a great potential as a high-rate cathode material for LIBs.

Long-term cycle life of the cathode material is a key for battery applications. To evaluate the cycling stability, the cyclic performance of FGNS is illustrated in comparison with the GO and GNS at a current density of 0.05 A $g^{-1}$ in Fig. 6(e). As expected, GO and GNS electrodes show poor cycling performance. The obvious capacity fade of GO is observed upon cycling, and the capacity of GO decreased to 80 mA h $g^{-1}$ after 100 cycles. It is worth noting that the GNS electrode with few oxygen-containing functional groups delivers a low reversible capacity of no more than 20 mA h $g^{-1}$ upon cycling. By contrast, the FGNS electrode delivers a high reversible capacity of 286 mA h $g^{-1}$ after 300 cycles. The gradual rise in enhanced capacity upon cycling may be due in part to the gradual penetration of electrolyte into the porous structure that promotes the activation of electrode materials, as well as $Li^+$ conduction [23,59]. Such a sharp contrast of cyclic performance of three samples clearly reveals that the oxygenic functional groups play a key role in enhancing the electrochemical performance. The lacking of oxygenic functional groups results in the low specific capacity of GNS. On the other hand, GO with more oxygen content shows lack luster electrochemical performance compared with FGNS, which was mainly due to the low conductivity resulting from the excess oxygenic groups. These results conform to the previously reported energy storage mechanism that the oxygenic functional groups act as active sites for lithium storage ($\rangle C{=}O + Li^+ + e^- \leftrightarrow \rangle CO{-}O{-}Li$) [24]. Importantly, the reactions of this special energy storage mechanism are highly reversible, as a result, nearly no obvious capacity decay of the FGNS sample was observed over cycles. Therefore, the high reversible capacity of FGNS can be linked to the abundant oxygenic groups that act as some electrochemical sites of lithium ion storage according to the reversible Faradaic reactions. Additionally, the high structural stability of this designed carbon materials and the strong chemical covalent bonding of the surface functional groups on the FGNS could contribute to the outstanding cycling stability.

To further understand the advantages of FGNS as cathode material for superior battery performance, electrochemical impedance spectroscopy (EIS) was performed at a full charged state (4.5 V) after 5 cycles. The Nyquist plots are shown in Fig. 6(f). As can be seen, all the plots exhibit one semicircle and one slope, which is a collective response of the kinetic process of active materials reaction with lithium [60]. The internal resistance ($R_s$) is the sum of the resistance of electrolyte, the active materials and the contact resistance between active material and current collector. The semicircle of the Nyquist plot corresponds to the interfacial charge transfer resistance ($R_{ct}$), and the slope in the low frequency region can be assigned to the solid state diffusion of the $Li^+$ ion in the electrodes [61,62]. The inset of Fig. 6(f) reveals an equivalent circuit used to fit

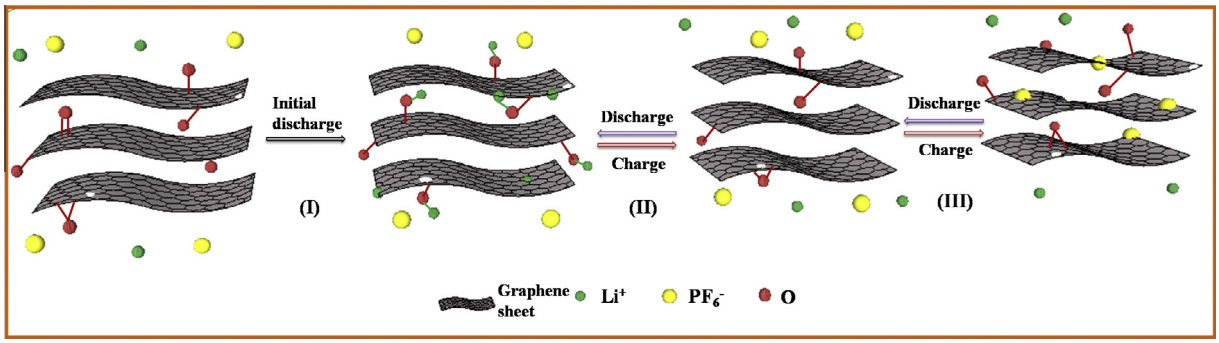


**Fig. 7.** Schematic illustration of the electrical energy storage mechanism of functionalized graphene nanosheets cathodes.

the EIS curves to measure $R_s$ and $R_{ct}$, where CPE and $Z_w$ are the constant phase element and the Warburg impendence, respectively. The extracted data of $R_{ct}$ and $R_s$ is tabulated in Table 3. Clearly, $R_s$ of all samples is less than 10 Ω, indicating that the electrolyte and contact resistance have neglectable effect on the electrochemical process of the cell. Surprisingly, there is a remarkable decrease from 2061 to 449.7 Ω for charge transfer resistance of GO and GNS. Thus, a sharp difference of $R_{ct}$ explains why GO shows poor performance, as we previously expected [36].

To analyze the effects of oxygen-containing groups and electrical conductivity on electrochemical performance intuitively, charge transfer resistance values and gravimetric discharge capacities as a function of the reduction degree are shown in Fig. 8, which were computed based on the data in Table 3 and Fig. 6(e). GO was first reduced to obtain FGNS, and FGNS was further reduced to obtain GNS. During these processes, oxygenic functional groups gradually decrease with the increase of reduction degree, which had been completely demonstrated from the aforementioned XPS and FT-IR results. The inset in Fig. 8 compares the dispersion of GO, FGNS and GNS into deionized water (0.5 mg $mL^{-1}$). It can be seen that GO maintains a stable dispersion with brown sight, indicating abundant oxygen functional groups on the GO surface. FGNS also shows good dispersion which is jet black, indicating the partial reduction of oxygen functional groups. It is due to electrostatic repulsions among anions ($COO^-$ and CO—$O^-$) on FGNS. Differently, GNS is gradually precipitated after the sonication process, indicating that GNS is hydrophobic due to few oxygenic functional groups. This is in good agreement with the XPS and FT-IR results. The decrease of charge transfer resistance with increasing reduction degree indicates the enhancement of electrical conductivity, which can be related to the removal of surface functional groups and the re-formation of the conjugated carbon $sp^2$ orbital on the graphene framework. In Fig. 8, observed high reversible capacity of the FGNS electrodes could be related to a larger amount of oxygenic functional groups on the graphene surface resulting from partial reduction (Fig. 4), while GO and GNS showed poor battery performance might be due to the inferior electrical conductivity and fewer oxygen functional groups, respectively. It can be concluded that FGNS with considerable oxygen-containing groups simultaneously shows relatively fast charge transfer and acceptable electrical conductivity, which might contribute to the excellent performance.

To further verify the superior cycling stability of the FGNS, we have carried out SEM measurements of the GO and GNS electrodes after 100 cycles (Fig. S3) and FGNS electrode after 150 cycles (Fig. S4(c and d)) at 0.05 A $g^{-1}$. The SEM images of FGNS electrode before cycling are present in Fig. S4(a and b). As can be seen, an intense aggregation occur in GO electrode (Fig. S3(a and b)), resulting in poor battery performance. By contrast, after repeated lithium insertion/extraction, the FGNS electrode after 150 cycles (Fig. S4(c and d)) show slight aggregation, but the 3D interconnected porous network nanostructure can still be retained when compared with the pristine FGNS electrode (Fig. S4(a and b)), indicating the stability of morphology and surface. It was considered to contribute to the superior cycling stability. In addition, though the GNS electrode after cycling show similar morphology with that of FGNS electrode, the inferior capacity of GNS further confirms the important role of oxygenic functional groups. In addition, ex-situ FT-IR provides some evidences of the superior cycling stability of the FGNS. As shown in Fig. S5, the presence of oxygenic functional groups (such as CO—OH and CO—O) in both of the FGNS cathodes before and after 150 charge/discharge cycles indicate that no obvious functional groups change of the FGNS electrode occurs after long-time cycling. This further demonstrates the superior cycling stability of the FGNS with abundant oxygenic functional groups function as lithium storage active sites. It is worth noting that the sample after 150 charge/discharge cycles reveals weaker C=O stretching absorption while the intensity of the C—O stretching absorption enhances, indicating that the double bonds of C=O functional groups were broken and the single bonds between carbon and oxygen were formed during lithium storage process.

In view of the high reversible capacity and excellent cycling stability of the designed FGNS cathode, we compared the electrochemical performance of the traditional cathode materials (commercialization and in research) with the designed FGNS, as shown in Table 4. It can be seen that the FGNS show higher specific capacity and better cycling performance than those current cathode materials. These high performance characteristics are urgently needed for building high performance cathode materials for LIBs. Therefore, this proposed FGNS may hold great promise for the development of high performance lithium ion batteries.

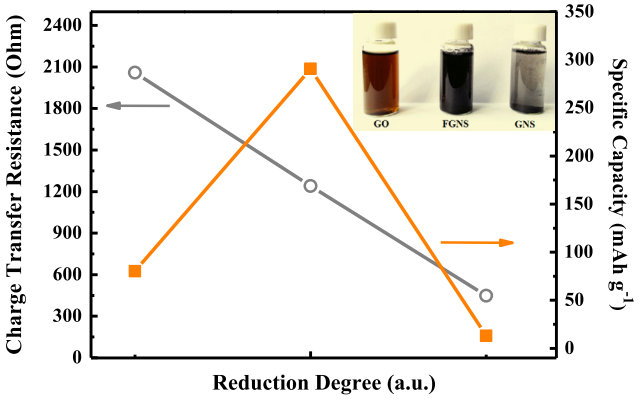


**Fig. 8.** Charge transfer resistance values after 5 cycles and gravimetric discharge capacities of the 100th cycle as a function of the reduction degree, as obtained from Table 3 and Fig. 6(e). Inset of the figure is the optical images of GO, FGNS and GNS solutions after sonication for 15 min.

**Table 3**
The typical fitted parameters in the electrochemical impedance spectroscopy.

| Samples | GO | FGNS | GNS |
|---|---|---|---|
| $R_s$ (Ω) | 9.113 | 1.774 | 4.871 |
| $R_{ct}$ (Ω) | 2061 | 1242 | 449.7 |

**Table 4**
Comparison of the electrochemical performance of the traditional cathode materials and this work.

| Cathode materials | Capacity (mA h $g^{-1}$) After *n*th cycle | Current density | Ref. |
|---|---|---|---|
| $LiCoO_2$ | ~115 (14th) | 1000 mA $g^{-1}$ | [63] |
| $LiMn_2O_4$ | ~85 (100th) | 148 mA $g^{-1}$ | [64] |
| $LiFePO_4$ | ~96 (30th) | 42.5 mA $g^{-1}$ | [65] |
| $LiFePO_4$ | ~104 (100th) | 17 mA $g^{-1}$ | [66] |
| $LiNi_{0.81}Co_{0.1}Al_{0.09}O_2$ | ~148 (200th) | 1 C | [67] |
| $LiNi_{0.5}Co_{0.2}Mn_{0.3}O_2$ | ~142 (50th) | 110 mA $g^{-1}$ | [68] |
| FGNS | ~286 (300th) | 50 mA $g^{-1}$ | This work |

## 4. Conclusions

In summary, we have developed a facile strategy to fabricate typical poriferous FGNS. When employed as a cathode material for LIBs, the FGNS framework exhibits a high reversible capacity, excellent cycling performance, and superior rate capability. The outstanding electrochemical performance of FGNS is attributed to the unique features of graphene based framework, including surface oxygen-containing functional groups functioning as reversible

redox reactions accompanied by the association and disassociation of $Li^+$, 3D poriferous conducting network which provides highly conductive transfer channels for efficient electron and Li-ion transport, easy accessibility for electrolyte infiltration and high specific surface area to adsorb Li-ions. This development of novel metal-free cathode materials provides a possibility to design high performance LIBs. More importantly, our study revealed that the structural stability as well as the strong chemical covalent bonding of the surface functional groups of FGNS were the main reasons that contribute to the outstanding cycling stability. Additionally, the tradeoff of the amount of oxygenic functional groups on FGNS signally affects the electrochemical performance. Therefore, we have developed a novel scalable route to design new cathode materials, and the revealed results will promote the development and optimizing of the novel graphene cathode for LIBs.

## Acknowledgments

This research was supported by the National Natural Science Foundation of China (51572194), the Key Projects of Tianjin Municipal Natural Science Foundation of China (14JCZDJC32200), Academic Innovation Funding of Tianjin Normal University (52XC1404), LPMT (Laboratory of Precision Manufacturing Technology), CAEP (China Academy of Engineering Physics) (KF14006), Training Plan of Leader Talent of University in Tianjin, Scientific Research Foundation for Returned Overseas Chinese Scholars of State Education Ministry, and the program of Thousand Youth Talents in Tianjin of China.

## Appendix A. Supplementary material

Supplementary data associated with this article can be found, in the online version, at http://dx.doi.org/10.1016/j.apenergy.2016.03.105.

## References

[1] Dunn B, Kamath H, Tarascon JM. Electrical energy storage for the grid: a battery of choices. Science 2011;334:928–35.
[2] Larcher D, Tarascon JM. Towards greener and more sustainable batteries for electrical energy storage. Nat Chem 2015;7:19–29.
[3] Hu C, Jain G, Tamirisa P, Gorka T. Method for estimating capacity and predicting remaining useful life of lithium-ion battery. Appl Energy 2014;126:182–9.
[4] Pearre NS, Swan LG. Technoeconomic feasibility of grid storage: mapping electrical services and energy storage technologies. Appl Energy 2015;137:501–10.
[5] Bruce PG, Scrosati B, Tarascon JM. Nanomaterials for rechargeable lithium batteries. Angew Chem Int Ed Engl 2008;47:2930–46.
[6] Martin C. Driving change in the battery industry. Nat Nanotechnol 2014;9:327–8.
[7] Luo X, Wang J, Dooner M, Clarke J. Overview of current development in electrical energy storage technologies and the application potential in power system operation. Appl Energy 2015;137:511–36.
[8] Ji L, Lin Z, Alcoutlabi M, Zhang X. Recent developments in nanostructured anode materials for rechargeable lithium-ion batteries. Energy Environ Sci 2011;4:2682–99.
[9] Simon P, Gogotsi Y, Dunn B. Materials science. Where do batteries end and supercapacitors begin? Science 2014;343:1210–1.
[10] Hu M, Pang X, Zhou Z. Recent progress in high-voltage lithium ion batteries. J Power Sources 2013;237:229–42.
[11] Jiang M, Key B, Meng YS, Grey CP. Electrochemical and structural study of the layered, "Li-Excess" lithium-ion battery electrode material $Li[Li_{1/9}Ni_{1/3}Mn_{5/9}]O_2$. Chem Mater 2009;21:2733–45.
[12] Jo M, Noh M, Oh P, Kim Y, Cho J. A new high power $LiNi_{0.81}Co_{0.1}A_{l0.09}O_2$ cathode material for lithium-ion batteries. Adv Energy Mater 2014;4. 1301583.
[13] Pan C-C, Banks CE, Song W-X, Wang C-W, Chen Q-Y, Ji X-B. Recent development of $LiNi_xCo_yMn_zO_2$: impact of micro/nano structures for imparting improvements in lithium batteries. Trans Nonf Met Soc China 2013;23:108–19.
[14] Luo D, Li G, Fu C, Zheng J, Fan J, Li Q, et al. A new spinel-layered Li-rich microsphere as a high-rate cathode material for Li-ion batteries. Adv Energy Mater 2014;4. 1400062.
[15] Hu G, Liu W, Peng Z, Du K, Cao Y. Synthesis and electrochemical properties of $LiNi_{0.8}Co_{0.15}Al_{0.05}O_2$ prepared from the precursor $Ni_{0.8}Co_{0.15}Al_{0.05}OOH$. J Power Sources 2012;198:258–63.
[16] Yang X, Wang X, Wei Q, Shu H, Liu L, Yang S, et al. Synthesis and characterization of a Li-rich layered cathode material $Li_{1.15}[(Mn_{1/3}Ni_{1/3}Co_{1/3})_{0.5}(Ni_{1/4}Mn_{3/4})_{0.5}]_{0.85}O_2$ with spherical core–shell structure. J Mater Chem 2012;22:19666–72.
[17] Fang Y, Lv Y, Che R, Wu H, Zhang X, Gu D, et al. Two-dimensional mesoporous carbon nanosheets and their derived graphene nanosheets: synthesis and efficient lithium ion storage. J Am Chem Soc 2013;135:1524–30.
[18] Bonaccorso F, Colombo L, Yu G, Stoller M, Tozzini V, Ferrari AC, et al. 2D materials. Graphene, related two-dimensional crystals, and hybrid systems for energy conversion and storage. Science 2015;347:1246501.
[19] Sun Y, Wu Q, Shi G. Graphene based new energy materials. Energy Environ Sci 2011;4:1113–32.
[20] Li X, Chen Y, Cheng Z, Jia L, Mo S, Liu Z. Ultrahigh specific surface area of graphene for eliminating subcooling of water. Appl Energy 2014;130:824–9.
[21] Wang H, Guan C, Wang X, Fan HJ. A high energy and power Li-ion capacitor based on a $TiO_2$ nanobelt array anode and a graphene hydrogel cathode. Small 2015;11:1470–7.
[22] Mo R, Lei Z, Rooney D, Sun K. Facile synthesis of nanocrystalline $LiFePO_4$/graphene composite as cathode material for high power lithium ion batteries. Electrochim Acta 2014;130:594–9.
[23] Su Y, Liu Y, Liu P, Wu D, Zhuang X, Zhang F, et al. Compact coupled graphene and porous polyaryltriazine-derived frameworks as high performance cathodes for lithium-ion batteries. Angew Chem Int Ed Engl 2015;54:1812–6.
[24] Jang BZ, Liu C, Neff D, Yu Z, Wang MC, Xiong W, et al. Graphene surface-enabled lithium ion-exchanging cells: next-generation high-power energy storage devices. Nano Lett 2011;11:3785–91.
[25] Byon HR, Gallant BM, Lee SW, Shao-Horn Y. Role of oxygen functional groups in carbon nanotube/graphene freestanding electrodes for high performance lithium batteries. Adv Funct Mater 2013;23:1037–45.
[26] Ha SH, Jeong YS, Lee YJ. Free standing reduced graphene oxide film cathodes for lithium ion batteries. ACS Appl Mater Interf 2013;5:12295–303.
[27] Lee SW, Gallant BM, Lee Y, Yoshida N, Kim DY, Yamada Y, et al. Self-standing positive electrodes of oxidized few-walled carbon nanotubes for light-weight and high-power lithium batteries. Energy Environ Sci 2012;5:5437–44.
[28] Lee SW, Yoshida N, Gallant BM, Chem S, Kim BS, Horn YS, et al. High-power lithium batteries from functionalized carbon-nanotube electrodes. Nat Nanotechnol 2010;5:531–7.
[29] Bachman JC, Kavian R, Graham DJ, Kim DY, Noda S, Nocera DG, et al. Electrochemical polymerization of pyrene derivatives on functionalized carbon nanotubes for pseudocapacitive electrodes. Nat Commun 2015;6:7040.
[30] Kim SY, Hong J, Kavian R, Lee SW, Hyder MN, Shao-Horn Y, et al. Rapid fabrication of thick spray-layer-by-layer carbon nanotube electrodes for high power and energy devices. Energy Environ Sci 2013;6:888.
[31] Lee SW, Gallant BM, Byon HR, Hammond PT, Shao-Horn Y. Nanostructured carbon-based electrodes: bridging the gap between thin-film lithium-ion batteries and electrochemical capacitors. Energy Environ Sci 2011;4:1972.
[32] Huang W, Zhu Z, Wang L, Wang S, Li H, Tao Z, et al. Quasi-solid-state rechargeable lithium-ion batteries with a calix[4]quinone cathode and gel polymer electrolyte. Angew Chem Int Ed Engl 2013;52:9162–6.
[33] Han X, Chang C, Yuan L, Sun T, Sun J. Aromatic carbonyl derivative polymers as high-performance Li-ion storage materials. Adv Mater 2007;19:1616–21.
[34] Byon HR, Lee SW, Chen S, Hammond PT, Shao-Horn Y. Thin films of carbon nanotubes and chemically reduced graphenes for electrochemical micro-capacitors. Carbon 2011;49:457–67.
[35] Ai W, Du Z, Fan Z, Jiang J, Wang Y, Zhang H, et al. Chemically engineered graphene oxide as high performance cathode materials for Li-ion batteries. Carbon 2014;76:148–54.
[36] Xiong D, Li X, Shan H, Yan B, Dong L, Cao Y, et al. Controllable oxygenic functional groups of metal-free cathodes for high performance lithium ion batteries. J Mater Chem A 2015;3:11376–86.
[37] Fan Z, Zhao Q, Li T, Yan J, Ren Y, Feng J, et al. Easy synthesis of porous graphene nanosheets and their use in supercapacitors. Carbon 2012;50:1699–703.
[38] Zhu Y, Murali S, Stoller MD, Ganesh KJ, Cai W, Ferreira PJ, et al. Carbon-based supercapacitors produced by activation of graphene. Science 2011;332:1537–41.
[39] Xu Y, Lin Z, Zhong X, Papandrea B, Huang Y, Duan X. Solvated graphene frameworks as high-performance anodes for lithium-ion batteries. Angew Chem Int Ed Engl 2015;54:5345–50.
[40] Lian P, Zhu X, Liang S, Li Z, Yang W, Wang H. Large reversible capacity of high quality graphene sheets as an anode material for lithium-ion batteries. Electrochim Acta 2010;55:3909–14.
[41] Ferrari AC, Meyer JC, Scardaci V, Casiraghi C, Lazzeri M, Mauri F, et al. Raman spectrum of graphene and graphene layers. Phys Rev Lett 2006;97:187401.
[42] Ferrari AC. Raman spectroscopy of graphene and graphite: disorder, electron–phonon coupling, doping and nonadiabatic effects. Solid State Commun 2007;143:47–57.
[43] Botas C, Álvarez P, Blanco C, Santamaría R, Granda M, Gutiérrez MD, et al. Critical temperatures in the synthesis of graphene-like materials by thermal exfoliation–reduction of graphite oxide. Carbon 2013;52:476–85.
[44] Chen YR, Chiu KF, Lin HC, Hsieh CY, Tsai CB, Chu BTT. The effect of dispersion status with functionalized graphenes for electric double-layer capacitors. Mater Sci Eng B 2014;190:59–65.

[45] Wang J, Wang HS, Wang K, Wang FB, Xia XH. Ice crystals growth driving assembly of porous nitrogen-doped graphene for catalyzing oxygen reduction probed by in situ fluorescence electrochemistry. Sci Rep 2014;4:6723.
[46] Gu W, Peters N, Yushin G. Functionalized carbon onions, detonation nanodiamond and mesoporous carbon as cathodes in Li-ion electrochemical energy storage devices. Carbon 2013;53:292–301.
[47] Ye M, Dong Z, Hu C, Cheng H, Shao H, Chen N, et al. Uniquely arranged graphene-on-graphene structure as a binder-free anode for high-performance lithium-ion batteries. Small 2014;10:5035–41.
[48] Liu Y, Deng R, Wang Z, Liu H. Carboxyl-functionalized graphene oxide–polyaniline composite as a promising supercapacitor material. J Mater Chem 2012;22:13619.
[49] Pan N, Guan D, Yang Y, Huang Z, Wang R, Jin Y, et al. A rapid low-temperature synthetic method leading to large-scale carboxyl graphene. Chem Eng J 2014;236:471–9.
[50] Ju H-M, Huh SH, Choi S-H, Lee H-L. Structures of thermally and chemically reduced graphene. Mater Lett 2010;64:357–60.
[51] Di Blasi O, Briguglio N, Busacca C, Ferraro M, Antonucci V, Di Blasi A. Electrochemical investigation of thermically treated graphene oxides as electrode materials for vanadium redox flow battery. Appl Energy 2015;147:74–81.
[52] Acik M, Lee G, Mattevi C, Pirkle A, Wallace RM, Chhowalla M, et al. The role of oxygen during thermal reduction of graphene oxide studied by infrared absorption spectroscopy. J Phys Chem C 2011;115:19761–81.
[53] Jaramillo J, Álvarez PM, Gómez-Serrano V. Oxidation of activated carbon by dry and wet methods. Fuel Process Technol 2010;91:1768–75.
[54] Chen H, Armand M, Demailly G, Tarascon JM. From biomass to a renewable $Li_xC_6O_6$ organic electrode for sustainable Li-ion batteries. ChemSusChem 2008;1:348–55.
[55] Xiong D, Li X, Shan H, Zhao Y, Dong L, Xu H, et al. Oxygen-containing functional groups enhancing electrochemical performance of porous reduced graphene oxide cathode in lithium ion batteries. Electrochim Acta 2015;174:762–9.
[56] Sakaushi K, Nickerl G, Wisser FM, Nishio-Hamane D, Hosono E, Zhou H, et al. An energy storage principle using bipolar porous polymeric frameworks. Angew Chem Int Ed Engl 2012;51:7850–4.
[57] Kim H, Lim HD, Kim SW, Hong J, Seo DH, Kim DC, et al. Scalable functionalized graphene nano-platelets as tunable cathodes for high-performance lithium rechargeable batteries. Sci Rep 2013;3:1506.
[58] Kim H, Park KY, Hong J, Kang K. All-graphene-battery: bridging the gap between supercapacitors and lithium ion batteries. Sci Rep 2014;4:5278.
[59] Wang D, Yang J, Li X, Geng D, Li R, Cai M, et al. Layer by layer assembly of sandwiched graphene/$SnO_2$ nanorod/carbon nanostructures with ultrahigh lithium ion storage properties. Energy Environ Sci 2013;6:2900.
[60] Osaka T, Momma T, Mukoyama D, Nara H. Proposal of novel equivalent circuit for electrochemical impedance analysis of commercially available lithium ion battery. J Power Sources 2012;205:483–6.
[61] Yan B, Li X, Bai Z, Li M, Dong L, Xiong D, et al. Superior lithium storage performance of hierarchical porous vanadium pentoxide nanofibers for lithium ion battery cathodes. J Alloys Compd 2015;634:50–7.
[62] Yan B, Li M, Li X, Bai Z, Dong L, Li D. Electrochemical impedance spectroscopy illuminating performance evolution of porous core–shell structured nickel/nickel oxide anode materials. Electrochim Acta 2015;164:55–61.
[63] Chen H, Grey CP. Molten salt synthesis and high rate performance of the "Desert-Rose" form of $LiCoO_2$. Adv Mater 2008;20:2206–10.
[64] Kim DK, Muralidharan P, Lee HW, et al. Spinel $LiMn_2O_4$ nanorods as lithium ion battery cathodes. Nano Lett 2008;8:3948–52.
[65] Jin B, Jin EM, Park KH, et al. Electrochemical properties of $LiFePO_4$-multiwalled carbon nanotubes composite cathode materials for lithium polymer battery. Electrochem Commun 2008;10:1537–40.
[66] Yang J, Wang J, Wang D, et al. 3D porous $LiFePO_4$/graphene hybrid cathodes with enhanced performance for Li-ion batteries. J Power Sources 2012;208:340–4.
[67] Jo M, Noh M, Oh P, et al. A new high power $LiNi_{0.81}Co_{0.1}Al_{0.09}O_2$ cathode material for lithium-ion batteries. Adv Energy Mater 2014;4. 1301583.
[68] Jung S K, Gwon H, Hong J, et al. Understanding the degradation mechanisms of $LiNi_{0.5}Co_{0.2}Mn_{0.3}O_2$ cathode material in lithium ion batteries. Adv Energy Mater 2014;4. 1300787.